(Received 23 September 2025, Accepted 3 December 2025, Scheduled 17 December 2025)

Miniaturized High-Efficiency Wideband Multi-Slot Antenna for Radar, Military, and 5G Applications for SDG-9

Swati V. Yadav[1,*], Manish V. Yadav[2], Himanshu Gupta[1], and Vikas Gupta[3]

[1] *Department of Instrumentation and Control Engineering*
Manipal Institute of Technology, Manipal Academy of Higher Education
Manipal, Karnataka 576104, India
[2] *Department of Aeronautical and Automobile Engineering*
Manipal Institute of Technology, Manipal Academy of Higher Education
Manipal, Karnataka 576104, India
[3] *Department of Electronics and Telecommunication Engineering*
Vidyavardhini's College of Engineering and Technology, Maharashtra, India

ABSTRACT: A compact wideband antenna with a multi-slot configuration is proposed for radar, military, and modern wireless communication systems. The antenna is fabricated on an FR-4 substrate with overall dimensions of $14 \times 16 \times 1.5\,\text{mm}^3$, corresponding to a miniaturized electrical size of $0.163\lambda \times 0.187\lambda \times 0.017\lambda_0$ at 3.5 GHz. To achieve broad impedance bandwidth and improved matching, multiple slots are etched on both the patch and ground surfaces. Experimental validation shows that the antenna effectively covers the 3.5–14 GHz frequency range, offering nearly 120% fractional bandwidth. Within this spectrum, it delivers a peak gain of 5.1 dB and a maximum radiation efficiency of about 89%, ensuring stable and low-loss performance. The compact structure maintains consistent radiation characteristics, making it suitable for portable and defense-oriented devices. Its ability to support Sub-6 GHz and 5G bands further enhances its applicability in next-generation communication platforms.

1. INTRODUCTION

The rapid advancement of wireless communication and defense technologies has significantly increased the demand for compact, wideband, and highly efficient antenna systems. Antennas are fundamental components in modern platforms, enabling seamless connectivity and reliable signal transmission across diverse frequency ranges. With the emergence of 5G and upcoming 6G networks, alongside military and aerospace communication requirements, antenna designs must offer broad bandwidth, high efficiency, and stable radiation characteristics within a compact size. Traditional antenna configurations often face limitations in achieving these combined features, especially when miniaturization and wideband coverage are simultaneously required.

Recent years have witnessed tremendous progress in antenna engineering, driven by the necessity to support multi-band communication, high data rates, and low latency. Defense and military systems demand antennas capable of operating under stringent conditions, offering robustness, low losses, and consistent performance across wide frequency spans. At the same time, the Sub-6 GHz band and millimeter-wave spectrum for 5G/6G applications require innovative designs that can deliver reliable coverage, high gain, and efficiency within a limited physical footprint. These demands highlight the importance of developing antennas that can integrate miniaturization with broadband operation.

This work presents a compact, high-efficiency antenna specifically designed to meet these challenges. The antenna achieves a wide operating band ranging from 2 to 14 GHz, with stable radiation patterns, a maximum gain of 5.1 dB, and radiation efficiency approaching 89%. Such performance ensures compatibility with defense communication, radar, surveillance, and next-generation wireless technologies, including 5G and 6G systems. The innovation lies in realizing broadband response and high efficiency within a reduced size, addressing the critical need for versatile, lightweight, and reliable antennas in modern communication infrastructures. The proposed design offers a practical solution where wideband operation, size reduction, and consistent performance are vital.

2. RELATED WORK

The advancement of wireless communication and defense technologies has created an urgent demand for compact, wideband, and highly efficient antenna designs. Microstrip patch antennas, in particular, have gained popularity due to their low profile, ease of fabrication, and adaptability to different frequency ranges. Considerable research has been carried out to address challenges related to bandwidth, gain, polarization, and miniaturization to meet the requirements of modern systems.

Mishra et al. [1] presented a detailed review on the parameters of microstrip patch antennas with different geometries and bandwidth enhancement techniques. Their study emphasized how structural modifications, slotting, and ground plane alter-

* Corresponding author: Swati Varun Yadav (yadav.swati@manipal.edu).

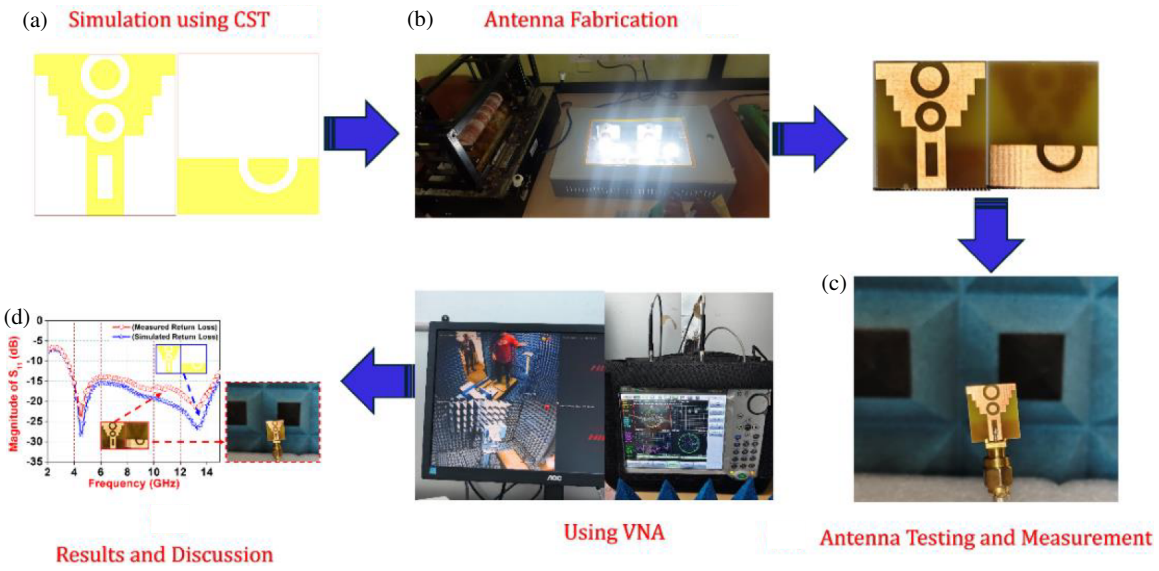

FIGURE 1. Graphical abstract. (a) Simulation in CST, (b) fabrication, (c) testing and measurement, and (d) comparison of simulated and measured results.

ations can significantly improve bandwidth and performance. This foundational work set the stage for further developments in designing antennas suitable for wideband and next-generation applications. Kurniawan and Mukhlishin [6] also highlighted the importance of wideband antenna design for modern communication systems, stressing the trade-offs between compact size and high performance.

In the context of 5G millimeter-wave communication, researchers have proposed numerous innovative designs. Przesmycki et al. [2] developed a broadband microstrip antenna operating at 28 GHz for 5G wireless systems, achieving stable radiation characteristics in high-frequency bands. Similarly, Imran et al. [3] demonstrated a millimeter-wave microstrip patch antenna designed specifically for 5G mobile communication, offering a compact structure suitable for portable devices. Verma et al. [8] proposed a small microstrip patch antenna optimized for future 5G applications, while Yadav et al. [15] introduced a cutting-edge antenna operating across S, C, and X bands for 5G and beyond, addressing the demand for multiband compatibility. Yadav et al. [18] designed a circular compact UWB antenna for 5G microwave applications, and Gupta et al. [19] proposed a TL-shaped circular parasitic planar antenna that further enhances bandwidth and compactness for 5G systems.

Several studies have also worked on bandwidth and radiation improvements. Khidre et al. [4] introduced a wideband dual-beam U-slot antenna with enhanced radiation characteristics. Baudha et al. [5] presented a U-shaped microstrip patch antenna with a partial ground plane designed for mobile satellite services, extending its relevance to satellite-based applications. Ghosh et al. [7] worked on improving polarization purity by employing a defected patch surface, demonstrating how structural modifications can suppress cross-polarization and improve antenna efficiency. Deshmukh et al. [12], Hota et al. [13], and Baudha et al. [14] investigated slot-loaded and uniquely shaped microstrip antennas, which effectively improved bandwidth and miniaturization without compromising radiation efficiency.

Beyond 5G, attention has shifted to 6G and terahertz communication bands, which promise ultra-high data rates and extremely low latency. Akyildiz et al. [9, 10] and Han and Chen [11] extensively studied propagation challenges and opportunities in millimeter-wave and terahertz frequency bands, outlining their potential role in future wireless networks. Their findings indicate that antenna designs capable of handling high path losses while maintaining efficiency are critical for 6G and beyond. Complementing these studies, Mazinani and Hassani [16] and Kim and Yun [17] proposed monopole antenna designs such as plate-loaded and inverted-L coupled strip configurations that achieved ultra-wideband characteristics, further extending applicability into next-generation systems.

Collectively, these works establish that microstrip antennas have evolved from narrowband, low-gain structures into highly optimized designs supporting wideband, Sub-6 GHz, 5G, and even 6G applications. The continuous focus on improving gain, radiation patterns, bandwidth, and efficiency, while keeping the antenna structure compact, ensures their relevance across military, satellite, and advanced wireless communication platforms.

Figure 1 illustrates the complete workflow adopted for the design, fabrication, and validation of the proposed antenna. The process begins with simulation and modeling using Computer Simulation Technology (CST) Microwave Studio (a), where the antenna geometry is optimized to achieve the required impedance bandwidth, gain, and efficiency. This step ensures that the theoretical design can support wideband operation while maintaining stable radiation characteristics. Once the optimized model is finalized, the next stage involves antenna fabrication in the laboratory (b). The structure is realized on an FR-4 substrate through conventional fabrication techniques, yielding a compact prototype with precise geometrical features.

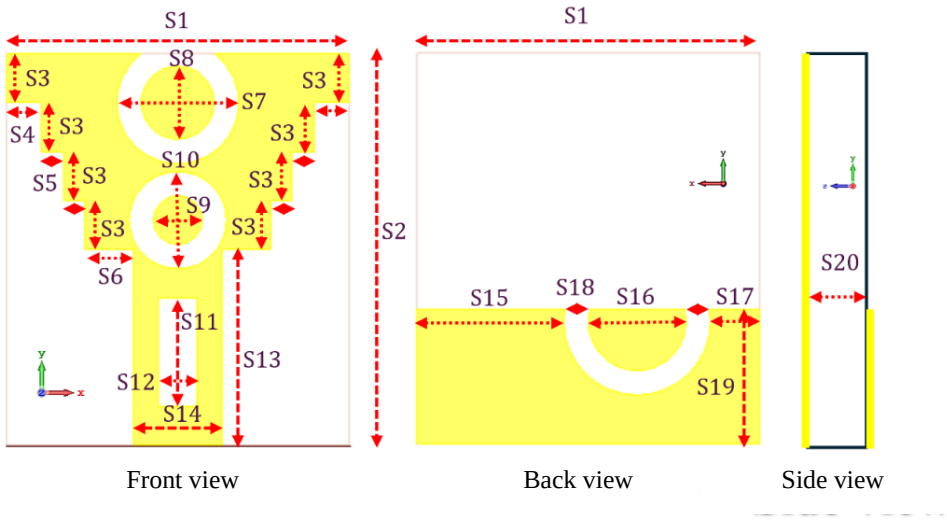

FIGURE 2. Conceptual design of an antenna.

TABLE 1. Parameters and values of the proposed antenna.

Parameters	S_1	S_2	S_3	S_4	S_5
Values (mm)	14	16	2	1.4	.5
Parameters	S_6	S_7	S_8	S_9	S_{10}
Values (mm)	1.4	5	2.5	1.5	3
Parameters	S_{11}	S12	S13	S14	S_{15}
Values (mm)	4.4	1.6	8	3.6	6
Parameters	S_{16}	S_{17}	S_{18}	S_{19}	S_{20}
Values (mm)	4	2.2	1	5.5	1.5

Following fabrication, the prototype undergoes testing and measurement (c) to validate its practical performance. A Vector Network Analyzer (VNA) and an anechoic chamber are employed to measure important parameters such as return loss, reflection coefficient, and impedance matching. Additionally, the antenna's radiation behavior is examined to verify its suitability for wideband communication applications. The final stage involves results and discussion (d), where the measured outcomes are compared with the simulated results. The comparative analysis shows close agreement between simulated and experimental data, confirming the accuracy of the design approach. This validation highlights that the antenna maintains its intended wideband characteristics, achieves high efficiency, and operates reliably under real-world conditions.

Overall, the graphical abstract demonstrates a systematic approach covering simulation, fabrication, measurement, and verification. It emphasizes the successful transition from theoretical design to practical implementation, ensuring that the proposed antenna delivers stable and efficient performance for applications in modern wireless systems such as 5G, sub-6 GHz, radar, and defense communications.

3. ANTENNA GEOMETRY AND EQUIVALENT CIRCUIT

The proposed planar antenna is designed with a compact structure featuring front, back, and side views. On the radiating side, circular slots and step-shaped edges are incorporated to improve impedance matching and extend bandwidth, while a modified feedline with a rectangular slot enhances current flow and return loss performance. On the reverse side, a defective ground plane with a semi-circular slot is introduced to suppress surface waves, thereby increasing both impedance bandwidth and radiation efficiency. The overall substrate thickness further contributes to bandwidth control and impedance characteristics. This miniaturized configuration makes the antenna well-suited for wideband applications, including next-generation communication, radar, and defense systems.

Figure 2 shows the geometry of the antenna, and its values are mentioned in Table 1. The substrate dimensions are $S_1 = 14\,\text{mm}$ (width) and $S_2 = 16\,\text{mm}$ (height). Step sections are defined by $S_3 = 2\,\text{mm}$, $S_4 = 1.4\,\text{mm}$, and $S_5 = 0.5\,\text{mm}$. Circular slots and their spacings are given by $S_6 = 1.4\,\text{mm}$, $S_7 = 5\,\text{mm}$, $S_8 = 2.5\,\text{mm}$, $S_9 = 1.5\,\text{mm}$, and $S_{10} = 3\,\text{mm}$. The feedline and associated slots are sized as $S_{11} = 4.4\,\text{mm}$, $S_{12} = 1.6\,\text{mm}$, $S_{13} = 8\,\text{mm}$, and $S_{14} = 3.6\,\text{mm}$. The defective ground structure is defined by $S_{15} = 6\,\text{mm}$, $S_{16} = 4\,\text{mm}$, $S_{17} = 2.2\,\text{mm}$, $S_{18} = 1\,\text{mm}$, and $S_{19} = 5.5\,\text{mm}$, while the substrate thickness is $S_{20} = 1.5\,\text{mm}$. Collectively, these parameters were optimized to achieve wide impedance bandwidth, compactness, and efficient radiation performance.

4. EQUIVALENT CIRCUIT MODEL

Figure 3 shows that the proposed antenna is modeled by a parallel resonant network connected to the feed. The feed (V_g, $Z = 50\,\Omega$) is connected through a small series matching network (L_m and C_m) to the antenna input node. From the antenna input node, multiple resonant branches are connected to ground: the main patch branch (modeled by an R-L-C series representing the dominant patch resonance), two circular slot resonators (top and bottom slots, each modeled as series R-L-C branches), and a U-shaped ground slot (modeled as a series R-L-C branch connected to ground). The substrate contributes a shunt capacitance from the feed node to ground (C_{sub}). Each

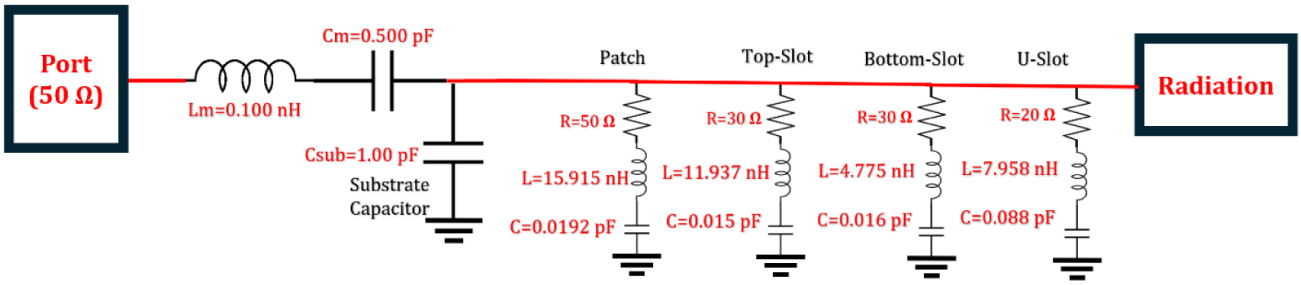

FIGURE 3. Equivalent circuit model.

resonator's R represents the combined radiation resistance and loss. The numeric component values below are initial estimates computed from assumed resonant frequencies and bandwidths using standard RLC relationships

$$L = Q * \frac{R}{\omega_0}; \quad C = \frac{1}{(\omega_0^2 * L)}; \quad Q = f_0/BW$$

Resonator	f_0 (GHz)	BW (GHz)	R (Ω)	L (nH)	C (pF)
Patch	9.100	0.500	50.00	15.9155	0.0192
Top slot	12.000	0.400	30.00	11.9366	0.0147
Bottom slot	18.000	1.000	30.00	4.7746	0.0164
U-slot	6.000	0.400	20.00	7.9577	0.0884

Series matching and substrate:
$L_m = 0.100$ nH, $C_m = 0.500$ pF, $C_{sub} = 1.000$ pF

5. ANTENNA CALCULATIONS

The antenna's electrical parameters were derived using standard formulas. The wavelength (λ) is calculated from $\lambda = \frac{c}{f}$

where c is the speed of light (3×10^8 m/s). At 3.5 GHz, the wavelength is 85.7 mm. Using the physical size of $14 \times 16 \times 1.5\,\text{mm}^3$, the electrical dimensions correspond to 0.163λ in length, 0.187λ in width, and 0.017λ in height, confirming a compact geometry relative to the operating wavelength. The impedance bandwidth percentage was evaluated as

$$BW\,(\%) = (f_{high} - f_{low})\,/f_{center} * 100$$

with $f_{low} = 3.5$ GHz, $f_{High} = 14$ GHz. The bandwidth is 120%, validating wideband capability.

5.1. Wavelength (λ) Calculation

$$\lambda = \frac{c}{f} = \frac{3 \times 10^8}{3.5 \times 10^9} = 85.7\,\text{mm}$$

Electrical Size = Physical Dimension/Wavelength (λ)
Antenna dimensions = 14 mm × 16 mm × 1.5 mm,
Length: $14/85.7 = 0.163\lambda$,
Width: $16/85.7 = 0.187\lambda$,
Height: $1.5/85.7 = 0.017\lambda$,
Electrical Size = $0.163\lambda \times 0.187\lambda \times 0.017\lambda$ (at 3.5 GHz).

5.2. Impedance Bandwidth (BW%)

$$BW\,(\%) = (f_{high} - f_{low})/f_{center} * 100$$
$$f_{low} = 3.5\,\text{GHz}, \quad f_{High} = 14\,\text{GHz}$$
$$f_{center} = \frac{3.5 + 14}{2} = 8.75\,\text{GHz}$$
$$BW\,(\%) = 120\%$$
$$ImpedanceBandwidth = 120\%$$

6. EVOLUTION OF THE ANTENNA

Figure 4 shows the design process of the antenna depicted in the figure progresses through four systematic stages, with each step introducing modifications that gradually enhance the performance and functionality of the structure. The highlighted yellow regions indicate the metallic portion of the antenna, while the white regions correspond to the etched-out sections, forming radiating and slot geometries.

The first stage begins with a simple rectangular substrate where the initial metallic layer is deposited. The left-hand section consists of a rectangular patch with a central slot forming a T-shaped geometry. On the right-hand side, the ground plane is partially covered with a rectangular metallic strip, leaving the upper region vacant. This basic configuration establishes the initial radiating element and the ground structure, which together provide the foundation for impedance matching and basic resonance characteristics. However, at this stage, the antenna has limited bandwidth and radiation efficiency due to its simplistic design. In the second stage, the radiating patch undergoes significant modifications. A stepped rectangular geometry is incorporated at the upper edges of the patch, producing multiple discontinuities that support higher-order modes and improve bandwidth. Additionally, circular and rectangular slots are etched at the center of the radiating patch. These slots play a critical role in introducing new resonances and enhancing impedance matching at multiple frequencies. The ground plane remains similar to Stage 1, with a partial rectangular metallic strip, maintaining a balance between radiation and isolation. At this point, the antenna begins to demonstrate multiband characteristics.

The third stage further optimizes the radiating patch by modifying the central slot arrangement. A circular slot is placed near the center, surrounding the previously created rectangular slot. This configuration increases current path lengths and

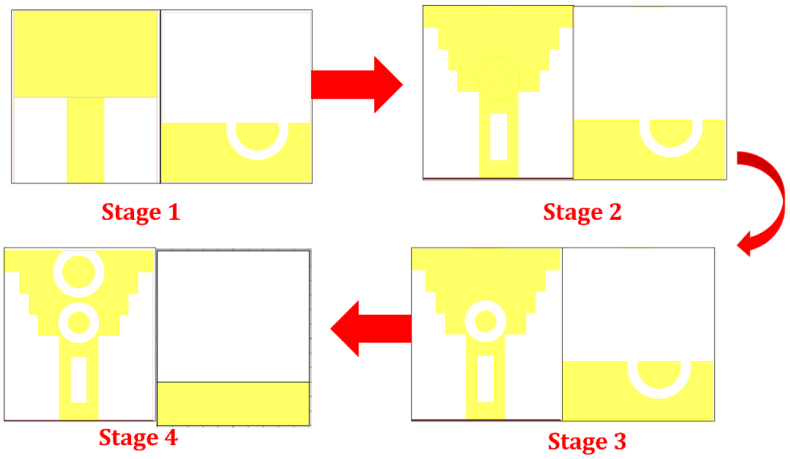

FIGURE 4. Antenna evolution from Stage 01–04.

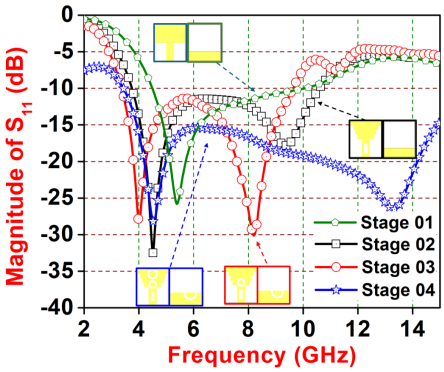

FIGURE 5. All stages S_{11} parameter from stage 01–04.

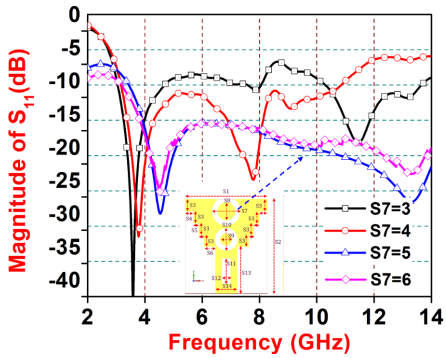

FIGURE 6. Simulated parameter sweep 'S_7'.

facilitates better tuning for desired frequency bands. On the ground plane side, a semicircular slot is introduced at the center of the metallic strip. This modification improves impedance bandwidth by redistributing surface currents and enhancing the coupling between the radiating patch and ground plane. The combined effect of these slots provides better control over resonance frequencies and improves radiation efficiency. The final stage presents a fully optimized design where multiple circular slots of varying diameters are embedded into the radiating patch. These slots create multiple current paths, allowing the antenna to operate efficiently across ultra-wideband or multi-frequency ranges. The stepped edges continue to support higher-order mode propagation, while the arrangement of slots ensures strong impedance matching over a broad spectrum. On the ground plane, the semicircular slot from Stage 3 is retained and optimized to complement the slot-loaded patch, ensuring reduced return loss and stable performance.

Figure 5 illustrates the simulated return loss S_{11} characteristics of the antenna across its four design stages, showing how structural modifications progressively improve performance. In Stage 1, the simple geometry provides limited bandwidth with a single resonance around 45 GHz, but poor impedance matching at higher frequencies. In Stage 2, the inclusion of stepped edges and a circular slot improves matching slightly and introduces multiple resonances, though the overall response remains less stable. In Stage 3, further structural refinements, including an additional slot and optimized ground configuration, enhance impedance bandwidth and create deeper resonances, particularly around 4.5 GHz and 8.5 GHz, indicating improved return loss. Finally, in Stage 4, the complete design with dual circular slots, stepped-edge geometry, and defected ground structure achieves the best performance, covering a wide operating range from about 3.5 GHz to beyond 14 GHz with multiple deep resonances, strong impedance matching, and improved bandwidth. This progressive improvement demonstrates the effectiveness of the step-by-step design methodology in achieving a compact, wideband antenna suitable for modern wireless communication applications.

7. RESULT AND DISCUSSION

Figure 6 shows the effect of varying parameter S_7 on the return loss characteristics of the antenna, with particular emphasis on the case of $S_7 = 5$ mm. When S_7 is set to 5 mm, the antenna achieves a wide operating bandwidth with multiple resonances, offering strong impedance matching across the frequency range of approximately 3.5 GHz to beyond 13 GHz.

The return loss dips below 20 dB at key frequencies, indicating efficient radiation and reduced reflection. Compared to other values of S_7, this configuration provides a more stable response with deeper resonances, ensuring better performance

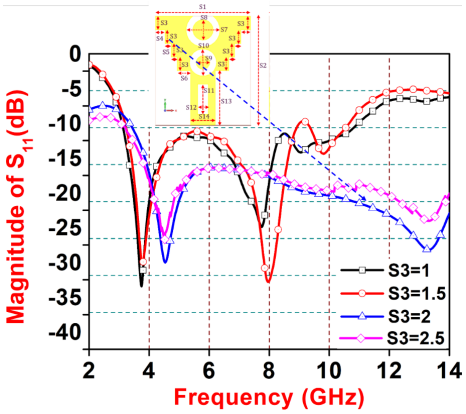

FIGURE 7. Simulated parameter sweep 'S_3'.

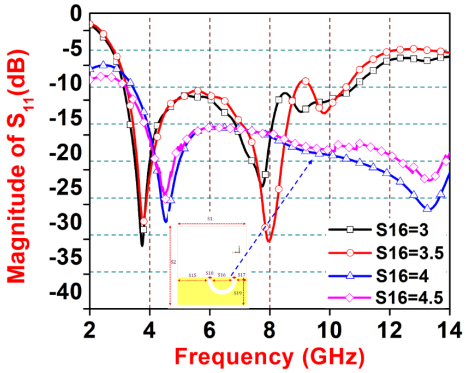

FIGURE 8. Simulated parameter sweep 'S_{16}'.

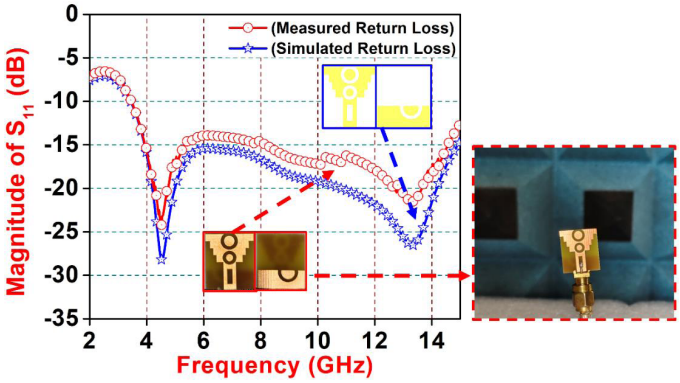

FIGURE 9. Comparison between simulated and measured S_{11} (reflection coefficient).

for ultra-wideband communication. Thus, $S_7 = 5$ mm is an optimized value that enhances both bandwidth and return loss, making the antenna more suitable for modern wireless applications requiring wide coverage and reliable impedance matching.

For the case of $S_3 = 2$ mm, the antenna demonstrates improved impedance matching and stable return loss across a wide frequency range, as shown in Figure 7. The response shows multiple deep resonances, particularly between 3.5 GHz and 13 GHz, where the return loss falls below 20 dB at several points, indicating efficient radiation and minimal signal reflection. Compared to lower values of S_3, this configuration provides better bandwidth coverage and stronger resonance depth, making it more suitable for ultra-wideband applications. Thus, with $S_3 = 2$ mm, the antenna achieves an optimized balance between bandwidth and resonance strength, ensuring reliable performance for modern high-frequency wireless communication systems.

For the configuration $S_{16} = 4$ mm, the antenna shows strong performance with multiple deep resonances and a broad operating bandwidth, as shown in Figure 8. The return loss response dips significantly below 20 dB across several frequency regions, particularly around 4 GHz, 6 GHz, and 13 GHz, indicating efficient impedance matching and reduced reflection. Compared to smaller values of S_{16}, this setting provides enhanced bandwidth coverage and deeper resonances, improving radiation efficiency across a wide range of frequencies. This makes the $S_{16} = 4$ mm configuration well-suited for wideband wireless applications, ensuring stable performance and reliable signal transmission.

To validate the consistency of the experimental outcomes, the antenna prototype was fabricated several times using a conventional chemical etching process. The performance of each fabricated sample remained highly consistent, with only minor variations observed across measurements. The measured discrepancies in gain (± 0.2 dB) and reflection coefficient ($\pm 3\%$) fall within acceptable limits and are primarily attributed to connector losses, slight misalignments, and setup-related variations. The strong agreement between repeated measurements and simulation results confirms the stability, repeatability, and robustness of the proposed antenna. This assessment enhances the experimental reliability and credibility of the presented findings.

The comparison of simulated and measured S_{11} results for the antenna within the frequency range of 3.5 to 14 GHz, shown in Figure 9, shows a strong correlation, confirming the accuracy of the proposed design. The antenna was fabricated in the laboratory using the chemical etching process, ensuring precise realization of the structure. Its performance was evaluated through testing and measurement carried out in an anechoic chamber using a Vector Network Analyzer (VNA) operating up to 40 GHz. Both simulated and experimental results display

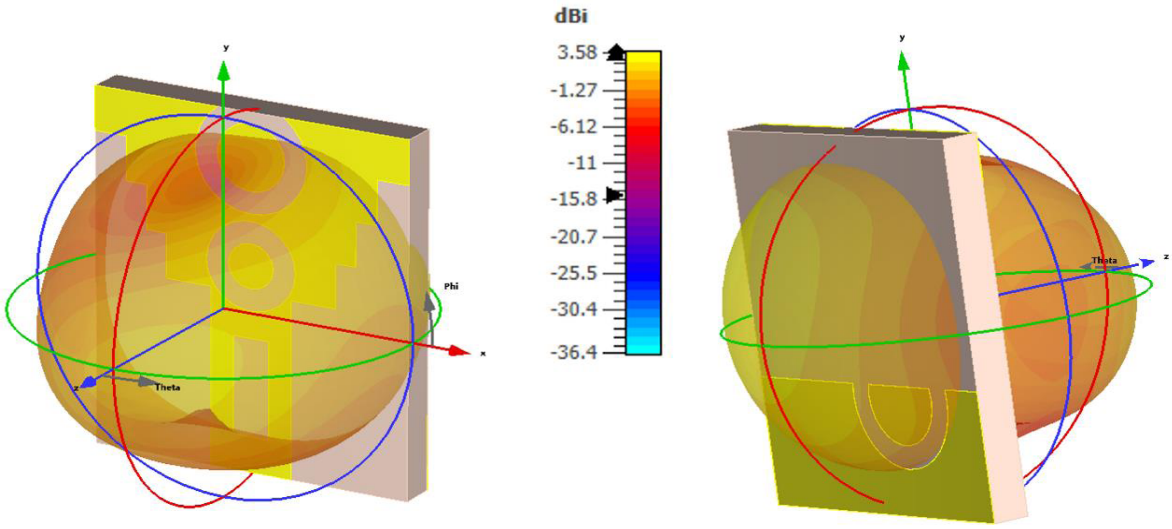

FIGURE 10. Radiation antenna 3-D lobe patterns at 4.5 GHz.

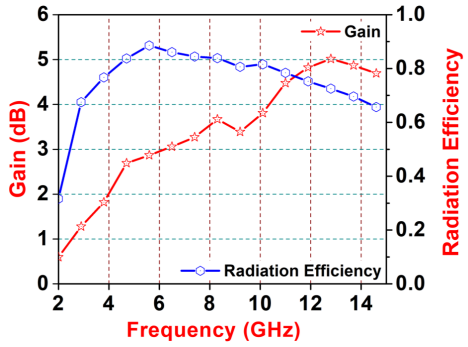

FIGURE 11. Peak gain and radiation efficiency of the antenna.

multiple resonances with return loss levels well below 10 dB across the operating band, confirming a wide impedance bandwidth. A fractional bandwidth of 120% is achieved with the central frequency of 8.75 GHz, making the antenna suitable for ultra-wideband applications. Minor variations between simulation and measurement can be attributed to fabrication tolerances, connector losses, and experimental conditions. Overall, the agreement between the two validates the reliability and practical applicability of the antenna for high-frequency wireless systems.

The 3D radiation patterns of the proposed antenna, as illustrated in Figure 10, show the distribution of radiated power across different directions. The radiation lobe exhibits a nearly omnidirectional behavior, ensuring good signal coverage in multiple orientations. The maximum gain reaches approximately 3.58 dBi, indicating efficient radiation performance for the designed frequency band. The plotted lobes confirm that the antenna provides stable radiation characteristics with minimal distortion, making it suitable for wideband wireless communication applications. The smooth and continuous radiation profile also suggests effective impedance matching and minimal back-lobe radiation, which enhances the overall efficiency of the antenna.

The plot presents the performance of the antenna in terms of gain and radiation efficiency across the 2–14 GHz frequency band, as shown in Figure 11. The gain gradually increases with frequency, achieving a maximum of about 5.1 dB, indicating effective signal amplification at higher frequencies. Similarly, the radiation efficiency follows a rising trend, starting near 0.35 and attaining a peak value close to 89%, after which it slightly declines to approximately 0.7 at 14 GHz. These results demonstrate that the antenna maintains a stable gain and high efficiency over a broad frequency range, confirming its suitability for wideband communication systems.

The surface current distributions of the proposed antenna at two resonant frequencies are illustrated in Figure 12. At 4.5 GHz (case A), the current flows are strongly concentrated around the circular radiating patches and the feed region, forming continuous loops that indicate the excitation of the fundamental resonance. The current spreads broadly across the structure, with higher intensities observed along the edges of the circular patches and at the junction between the feedline and radiators, where the maximum current density reaches approximately 40.1 dB (A/m). In contrast, at 13 GHz (case B), the current distribution becomes more localized and fragmented, with tighter loops mainly confined to the rims of the circular patches and the narrow junctions. The current direction exhibits rapid reversals, a typical feature of higher-order modes, while the maximum density slightly decreases to about 38.8 dB (A/m). These observations confirm that at lower frequencies the antenna operates in a fundamental mode with widespread current distribution, whereas at higher frequencies it supports higher-order modes with more confined and complex current paths, validating the antenna's multiband behavior.

The radiation performance of the proposed antenna at 4.5 GHz is shown in Figure 13, where both the H-plane and E-plane patterns are presented. In (a), the H-plane ($\theta = 0°$) exhibits an almost omnidirectional behavior, as the radiation pattern forms a nearly circular shape with uniform distribution in all azimuthal directions. This indicates that at 4.5 GHz, the antenna provides wide coverage in the horizontal plane, which is beneficial for applications requiring consistent radiation across different directions. In contrast, (b) shows the E-plane

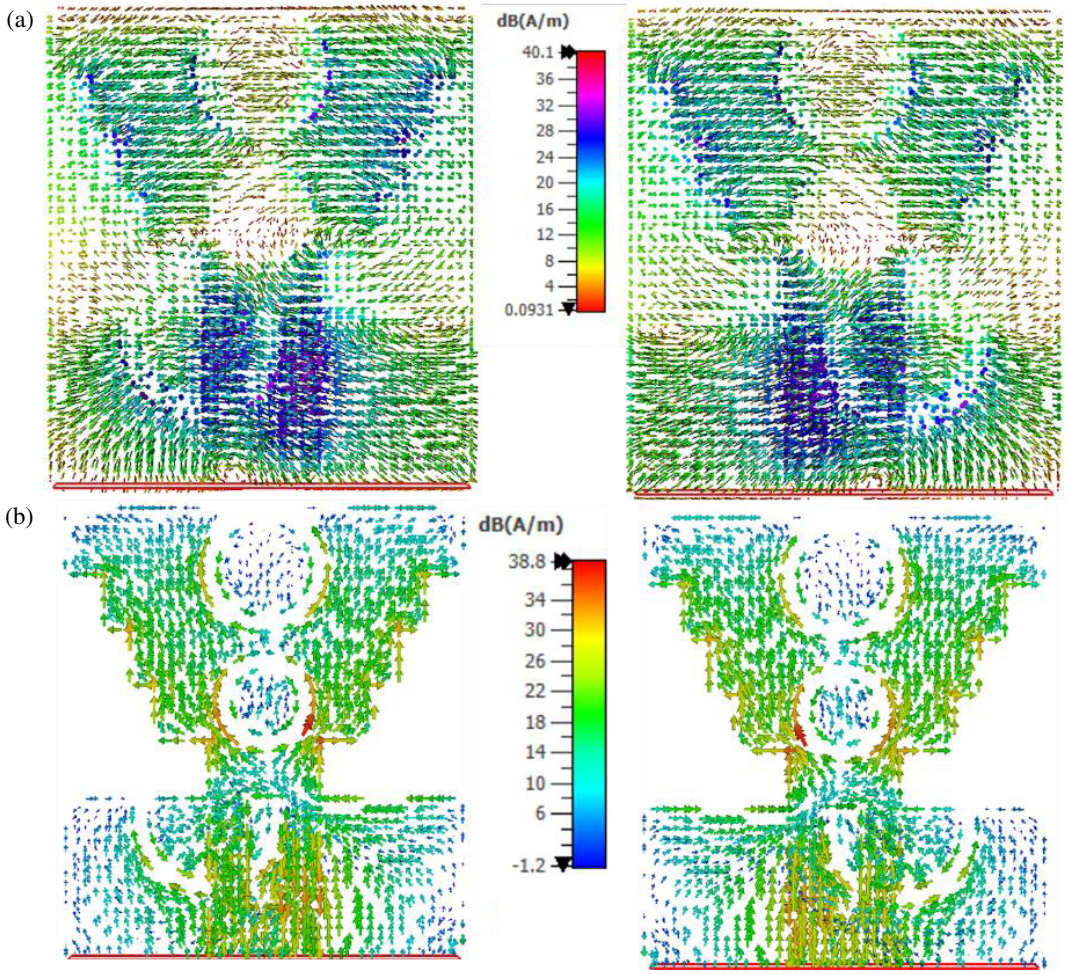

FIGURE 12. Surface current distribution of the antenna at (a) 4.5 GHz, (b) 13 GHz.

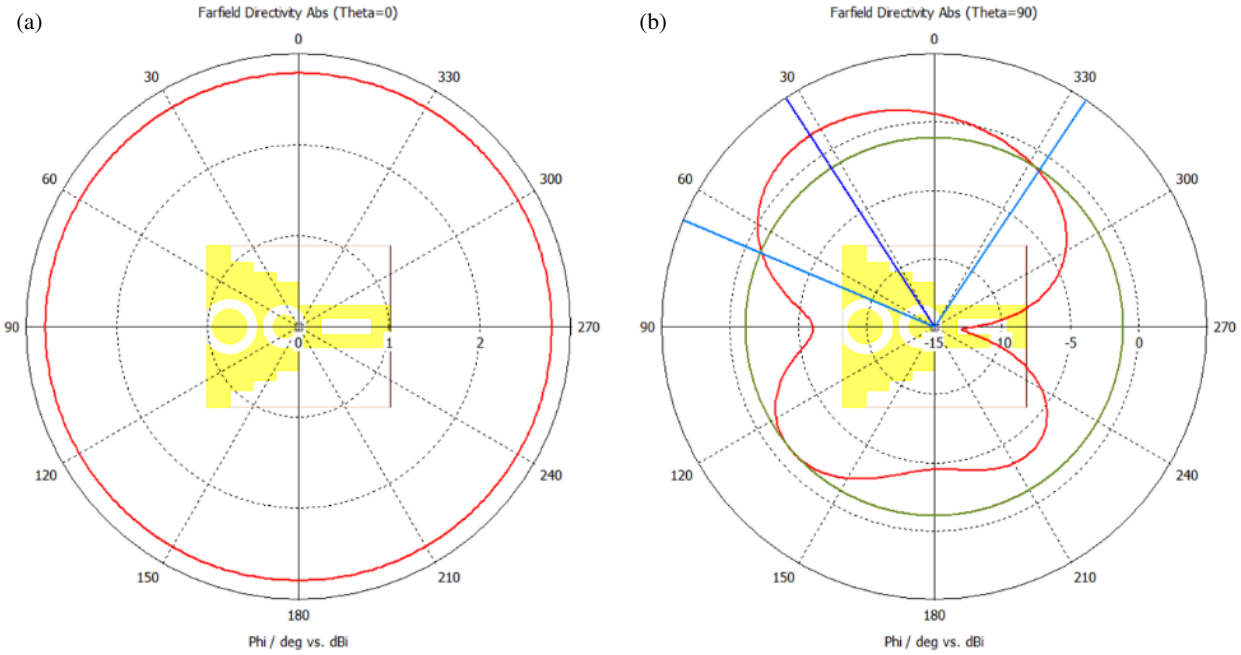

FIGURE 13. Radiation patterns of the antenna at 4.5 GHz, E-plane and H-plane.

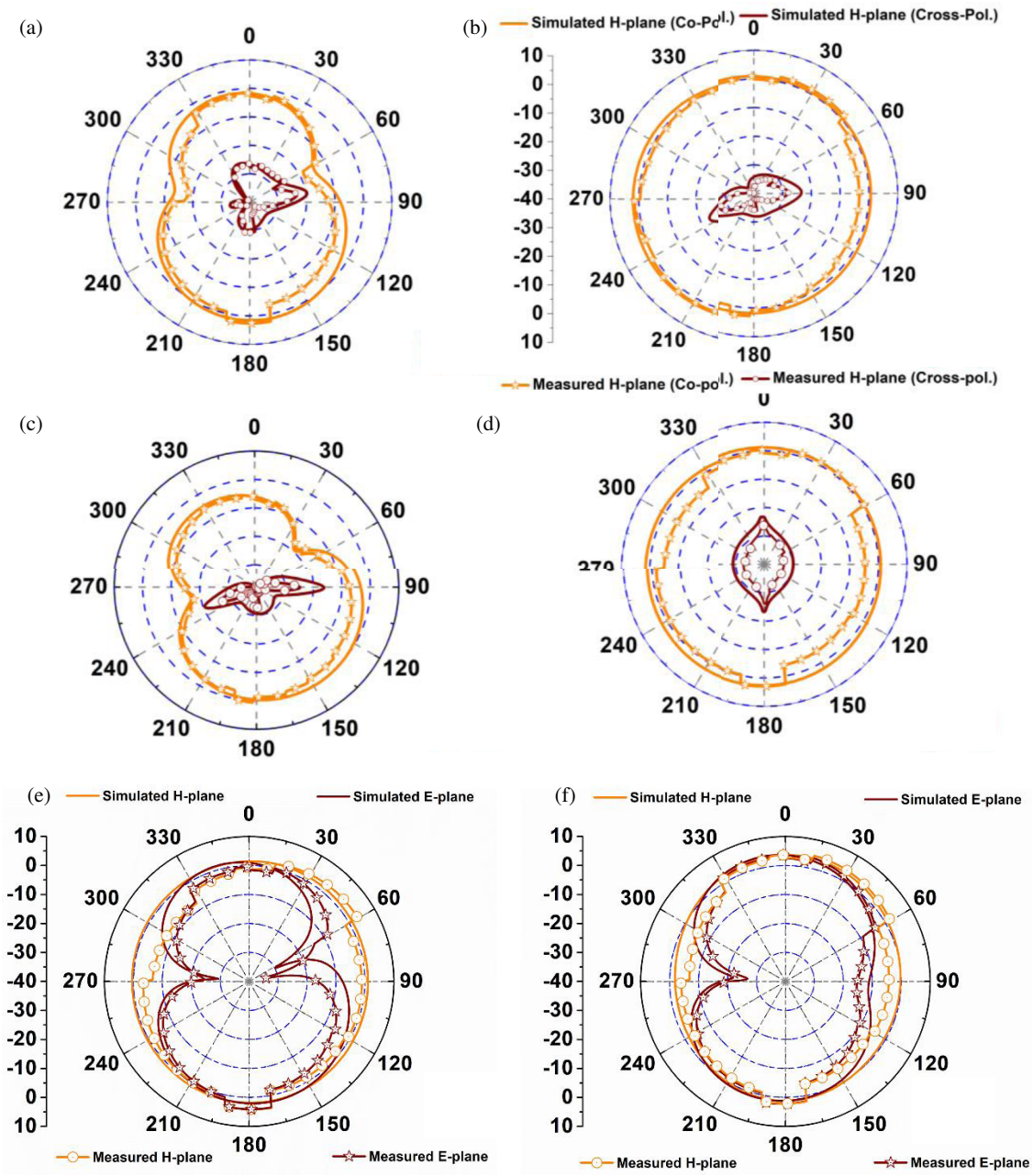

FIGURE 14. Simulated and measured H-plane radiation patterns of the proposed antenna at 5 GHz and 13 GHz. Figures (a) and (b) represent simulated results, while (c) and (d) show measured results. The co-polarized components dominate with significantly lower cross-polarization, ensuring stable radiation performance across both frequencies. (e) and (f) Simulated and measured radiation patterns of the proposed antenna at (e) 8 GHz and (f) 10 GHz.

($\theta = 90°$) pattern at the same frequency. Here, the radiation becomes more directive, with a well-defined main lobe accompanied by smaller side lobes and nulls. The main lobe directs energy effectively in a specific direction, while the side lobes represent minor radiation leakage due to higher-order mode excitation. The combination of these patterns confirms that at 4.5 GHz, the antenna achieves an omnidirectional H-plane for broad coverage and a directive E-plane for focused radiation, validating its suitability for multiband wireless applications.

Figure 14 shows that the radiation characteristics of the proposed antenna were analyzed in terms of co-polarization and cross-polarization at two distinct frequencies: 5 GHz and 13 GHz. At 5 GHz, the simulated (Fig. (a)) and measured (Fig. (c)) H-plane patterns show that the co-polarized component maintains a nearly omnidirectional behavior with good coverage across the angular range. The radiation is smooth and consistent, with the cross-polarized levels remaining significantly lower throughout, confirming strong polarization purity. This low cross-polarization indicates minimal unwanted radiation, thereby enhancing signal clarity and stability. Minor discrepancies between simulated and measured results can be attributed to fabrication tolerances and measurement setup, but the overall agreement is strong.

TABLE 2. Comparison table.

Reference/Work	Size (mm^3/mm^2)	Frequency Band (GHz)	IBW (%)	Gain (dB)	Efficiency (%)	Applications
[4]	$30 \times 35\,mm^2$	3–10	~ 107.7	8	88	Broadband radar
[5]	$25 \times 30\,mm^2$	1.5–4	~ 92.3	5	82	MSS/satellite
[6]	$30 \times 25\,mm^2$	2.5–8	~ 102.9	6.5	84	Wireless comm.
[7]	$28 \times 26\,mm^2$	2.8–7.5	~ 91.4	6.2	83	Polarization purity
[8]	$20 \times 15\,mm^2$	3.5–6	~ 55.6	4.8	81	Small 5G devices
[12]	$28 \times 22\,mm^2$	3–9	~ 100	6.1	85	Broadband
[13]	$20 \times 18\,mm^2$	3–11	~ 114.3	5.5	82	UWB, 5G
[14]	$22 \times 20\,mm^2$	2.5–9.5	~ 107.7	6.3	86	WiMAX, LTE
[15]	$18 \times 20\,mm^2$	2–12	~ 142.9	7.2	88	5G & beyond
[16]	$30 \times 28\,mm^2$	2.2–8.5	~ 110.6	5.2	82	Wideband
[17]	$25 \times 22\,mm^2$	3.1–10.6	~ 108.2	6.5	85	UWB
[18]	$15 \times 14\,mm^2$	3–14	~ 122.2	5.8	87	5G microwave
[19]	$16 \times 15\,mm^2$	4–12	~ 100	6.0	86	5G microwave
Proposed Design	$14 \times 16 \times 1.5\,mm^3$	3.5–14	120	5.1	89	Defense, radar, 5G

At 13 GHz, the radiation patterns (Fig. (b): simulated, Fig. (d): measured) again demonstrate that the co-polarized component is dominant, displaying good symmetry and stability. The cross-polarization levels are well suppressed, remaining far below the co-polarized values across most angular regions. This illustrates that even at higher frequencies, the antenna maintains excellent polarization discrimination. Such behavior ensures reliable performance in high-frequency applications, supporting enhanced bandwidth utilization and minimizing interference.

Figures 14 ((e) and (f)) illustrate the radiation characteristics of the proposed antenna at 8 GHz and 10 GHz, demonstrating stable and well-balanced performance in both the E-plane and H-plane. The H-plane exhibits an almost omnidirectional radiation pattern, ensuring uniform coverage across all azimuthal directions, an essential feature for wide-area communication systems. In contrast, the E-plane shows a bidirectional pattern with two dominant main lobes and minor side lobes, indicating good directivity and effective radiation control. The close agreement between simulated and measured results confirms the antenna's consistent performance and high reliability across the tested frequencies. Overall, these results verify that the antenna maintains stable radiation and polarization characteristics with minimal distortion at higher frequencies, making it well-suited for broadband, radar, and 5G communication applications.

The literature review in Table 2 highlights key developments in microstrip and planar antenna research, focusing on their role in modern wireless systems such as 5G and emerging 6G networks. A variety of innovative geometries, including U-slot, U-shaped, dumbbell-shaped, inverted-L, and semi-circular slot structures, have been explored to improve impedance bandwidth, gain, and radiation efficiency. These designs span a wide operating spectrum, from sub-6 GHz to millimeter-wave and terahertz frequencies, making them suitable for applications in wireless communication, radar, and satellite systems.

A consistent challenge evident across the reviewed works is achieving compact size while preserving wideband characteristics. Researchers have addressed this by employing slotting techniques, defected patch structures, and partial ground planes, which enhance bandwidth and impedance matching without significantly increasing antenna dimensions. Reported performance metrics indicate gains typically between 4–8 dB and efficiencies above 80%, demonstrating reliable low-loss operation. Notably, several studies achieved substantial impedance bandwidths, ranging from about 30% to more than 120%, showcasing the adaptability of these designs for future communication standards.

8. CONCLUSIONS

The developed antenna successfully combines miniaturization, broadband response, and high radiation efficiency in a single design. With compact dimensions of $14 \times 16 \times 1.5\,mm^3$, corresponding to an electrical size much smaller than one wavelength at 3.5 GHz, it offers a significantly reduced footprint. Experimental measurements verify a wide operational range from 3.5 to 14 GHz, achieving an impressive fractional bandwidth about 120%. Across this range, the antenna provides a peak gain of 5.1 dB and a radiation efficiency of nearly 89%, ensuring consistent and low-loss performance. These outcomes confirm that the multi-slot miniaturization approach effectively enhances bandwidth while maintaining strong radiation stability. The compact yet efficient configuration addresses one of the major design challenges in modern antenna technology. With these advantages, the proposed antenna is ideally suited for radar, surveillance, defense communication, and emerging 5G/6G wireless systems, enabling reliable and scalable communication performance.

REFERENCES

[1] Mishra, B., R. K. Verma, R. K. Singh, et al., "A review on microstrip patch antenna parameters of different geometry and bandwidth enhancement techniques," *International Journal of Microwave and Wireless Technologies*, Vol. 14, No. 5, 652–673, 2022.

[2] Przesmycki, R., M. Bugaj, and L. Nowosielski, "Broadband microstrip antenna for 5G wireless systems operating at 28 GHz," *Electronics*, Vol. 10, No. 1, 1, 2021.

[3] Imran, D., M. M. Farooqi, M. I. Khattak, Z. Ullah, M. I. Khan, M. A. Khattak, and H. Dar, "Millimeter wave microstrip patch antenna for 5G mobile communication," in *2018 International Conference on Engineering and Emerging Technologies (ICEET)*, 1–6, Lahore, Pakistan, Feb. 2018.

[4] Khidre, A., K.-F. Lee, A. Z. Elsherbeni, and F. Yang, "Wide band dual-beam U-slot microstrip antenna," *IEEE Transactions on Antennas and Propagation*, Vol. 61, No. 3, 1415–1418, 2013.

[5] Baudha, S., K. Kapoor, and M. V. Yadav, "U-shaped microstrip patch antenna with partial ground plane for mobile satellite services (MSS)," in *2019 URSI Asia-Pacific Radio Science Conference (AP-RASC)*, 1–5, New Delhi, India, Mar. 2019.

[6] Kurniawan, A. and S. Mukhlishin, "Wideband antenna design and fabrication for modern wireless communications systems," *Procedia Technology*, Vol. 11, 348–353, 2013.

[7] Ghosh, A., S. K. Ghosh, D. Ghosh, and S. Chattopadhyay, "Improved polarization purity for circular microstrip antenna with defected patch surface," *International Journal of Microwave and Wireless Technologies*, Vol. 8, No. 1, 89–94, 2016.

[8] Verma, S., L. Mahajan, R. Kumar, H. S. Saini, and N. Kumar, "A small microstrip patch antenna for future 5G applications," in *2016 5th International Conference on Reliability, Infocom Technologies and Optimization (Trends and Future Directions) (ICRITO)*, 460–463, Noida, India, Sep. 2016.

[9] Akyildiz, I. F., C. Han, and S. Nie, "Combating the distance problem in the millimeter wave and terahertz frequency bands," *IEEE Communications Magazine*, Vol. 56, No. 6, 102–108, Jun. 2018.

[10] Akyildiz, I. F., J. M. Jornet, and C. Han, "Terahertz band: Next frontier for wireless communications," *Physical Communication*, Vol. 12, 16–32, 2014.

[11] Han, C. and Y. Chen, "Propagation modeling for wireless communications in the terahertz band," *IEEE Communications Magazine*, Vol. 56, No. 6, 96–101, Jun. 2018.

[12] Deshmukh, A. A., D. Singh, P. Zaveri, M. Gala, and K. P. Ray, "Broadband slot cut rectangular microstrip antenna," *Procedia Computer Science*, Vol. 93, 53–59, 2016.

[13] Hota, S., M. V. Yadav, S. Baudha, and B. B. Mangaraj, "Miniaturized planar ultra-wideband patch antenna with semi-circular slot partial ground plane," in *2019 IEEE Indian Conference on Antennas and Propogation (InCAP)*, 1–4, Ahmedabad, India, 2019.

[14] Baudha, S., H. Garg, and M. V. Yadav, "Dumbbell shaped microstrip broadband antenna," *Journal of Microwaves, Optoelectronics and Electromagnetic Applications*, Vol. 18, 33–42, 2019.

[15] Yadav, M. V., S. V. Yadav, T. Ali, S. K. K. Dash, N. T. Hegde, and V. G. Nair, "A cutting-edge S/C/X band antenna for 5G and beyond application," *AIP Advances*, Vol. 13, 105123, 2023.

[16] Mazinani, S. M. and H. R. Hassani, "A novel broadband plate-loaded planar monopole antenna," *IEEE Antennas and Wireless Propagation Letters*, Vol. 8, 1123–1126, 2009.

[17] Kim, G.-H. and T.-Y. Yun, "Compact ultrawideband monopole antenna with an inverted-l-shaped coupled strip," *IEEE Antennas and Wireless Propagation Letters*, Vol. 12, 1291–1294, 2013.

[18] Yadav, S. V., M. V. Yadav, T. Ali, S. K. K. Dash, N. T. Hegde, and V. G. Nair, "A circular compact ultra-wideband antenna for 5G microwave applications," *TELKOMNIKA (Telecommunication Computing Electronics and Control)*, Vol. 22, No. 3, 556–566, 2024.

[19] Gupta, R., M. V. Yadav, and S. V. Yadav, "TL-shaped circular parasitic compact planar antenna for 5G microwave applications," in *International Conference on Electrical and Electronics Engineering*, 507–515, R. N. Shaw et al. (eds.), Springer, Singapore, 2024.